Cancer Cell
Article

Inactivation of the Deubiquitinase CYLD in Hepatocytes Causes Apoptosis, Inflammation, Fibrosis, and Cancer

Kostas Nikolaou,[1] Ageliki Tsagaratou,[1,2] Christina Eftychi,[1] George Kollias,[1] George Mosialos,[2] and Iannis Talianidis[1,*]
[1]Biomedical Sciences Research Center Alexander Fleming, 16672 Vari, Greece
[2]School of Biology, Aristotle University of Thessaloniki, 54124 Thessaloniki, Greece
*Correspondence: talianidis@fleming.gr
DOI 10.1016/j.ccr.2012.04.026

SUMMARY

The tumor suppressor cylindromatosis (CYLD) inhibits the NFκB and mitogen-activated protein kinase (MAPK) activation pathways by deubiquitinating upstream regulatory factors. Here we show that liver-specific disruption of CYLD triggers hepatocyte cell death in the periportal area via spontaneous and chronic activation of TGF-β activated kinase 1 (TAK1) and c-Jun N-terminal kinase (JNK). This is followed by hepatic stellate cell and Kupffer cell activation, which promotes progressive fibrosis, inflammation, tumor necrosis factor (TNF) production, and expansion of hepatocyte apoptosis toward the central veins. At later stages, compensatory proliferation results in the development of cancer foci featuring re-expression of oncofetal hepatic and stem cell-specific genes. The results demonstrate that, in the liver, CYLD acts as an important regulator of hepatocyte homeostasis, protecting cells from spontaneous apoptosis by preventing uncontrolled TAK1 and JNK activation.

INTRODUCTION

The nuclear factor (NF)-κB signaling pathway regulates multiple physiological and pathological processes, including immune responses and carcinogenesis (Vallabhapurapu and Karin, 2009). The principal regulatory step of NFκB-mediated signal transduction is the activation of IκB kinase (IKK), which phosphorylates members of the IκB family of inhibitory proteins that keep NFκB transcription factors inactive in the cytoplasm. The IKK complex consists of two catalytic subunits (IKK1 and IKK2) and the regulatory subunit (NEMO/IKKγ). It is interesting and pertinent to function that IKK activation by different receptor signals involves conjugation of K63-linked ubiquitin chains to several upstream regulatory components of the signaling cascade. These include the TNF receptor associated factors TRAF2 and TRAF6, the TGFβ-activated kinase TAK1, the receptor interacting protein RIP1 and NEMO (Sun, 2008; Chen, 2005). K63-linked poly-ubiquitin chains serve as interaction surfaces to facilitate the formation of stable TNFR1 core signaling complexes and/or act as modulators of the enzymatic activities of the modified factors (Chen, 2005; Sun, 2010). For example, poly-ubiquitination of TAK1 is required for its activity to phosphorylate IKK1 and IKK2 in their activation loops and trigger IκBα phosphorylation (Rincón and Davis, 2009; Sun, 2010).

The recent finding that K63-linked ubiquitination is a reversible reaction provides a strong indication that this modification represents an important layer of regulation in the process. The major enzyme that removes K63-linked polyubiquitin chains from NFκB pathway effectors is the cylindromatosis tumor suppressor CYLD (Trompouki et al., 2003; Brummelkamp et al., 2003; Kovalenko et al., 2003; Wright et al., 2007). Overexpression of CYLD in mammalian cells results in deubiquitination of NEMO and several upstream regulators like TRAF2, TRAF6, or TAK1 (Trompouki et al., 2003; Brummelkamp et al., 2003; Kovalenko et al., 2003; Yoshida et al., 2005). In addition, knockdown

Significance

Previous studies have revealed protumorigenic effects of genetic ablation of TAK1, NFκB essential modulator (NEMO), and IKKβ, suggesting that the NFκB signaling pathway plays a central role in the pathogenesis of hepatocellular carcinoma (HCC). The results presented here provide further insights into the mechanisms that link inflammation to cancer. In contrast to expectations, we found that liver-specific inactivation of CYLD leads to the development of HCC. CYLD deficiency triggers a multistep mechanism that mimics the major hallmarks of human HCC: hepatocyte death, inflammation, and fibrosis. The data suggest that controlling TAK1-induced downstream signaling cascades by the enzymatic activity of CYLD is critical for the maintenance of physiological liver homeostasis, as the final outcome of either inactivation or activation of the pathway is cancer.

or knockout of CYLD in different cell types leads to increased ubiquitination of these factors (Reiley et al., 2005; Zhang et al., 2006; Reiley et al., 2007). Together, these findings have established the view that CYLD is primarily a negative regulator of NFκB signaling.

CYLD was initially identified as a gene mutated in familial cylindromatosis that predisposes patients to the development of skin appendage tumors (Bignell et al., 2000). The broad role of CYLD in the regulation of cell survival and proliferation is highlighted by the downregulation of CYLD expression in several other types of human cancer, including colon cancer, lung cancer, multiple myeloma, and hepatocellular carcinoma (Zhong et al., 2007; Annunziata et al., 2007; Keats et al., 2007; Hellerbrand et al., 2007). Hepatocellular carcinoma (HCC) is the most common type of liver cancer, which in most cases develops in conjunction with chronic hepatitis or cirrhosis. Previous studies have revealed a major role of the NFκB signaling pathway in the mechanisms that link chronic inflammation to the pathogenesis of HCC (Maeda et al., 2005; Luedde et al., 2007; Bettermann et al., 2010; Luedde and Schwabe, 2011). Impediment of NFκB activation by disruption of *IKKβ* in the liver sensitized mice to diethylnitrosamine-induced hepatocarcinogenesis, while its deletion in both hepatocytes and Kupffer cells had the opposite effect (Maeda et al., 2005). Similarly, hepatocyte specific deletion of *NEMO* or *TAK1* in mice resulted in spontaneous development of hepatocellular carcinoma (Luedde et al., 2007; Inokuchi et al., 2010; Bettermann et al., 2010). As NFκB in most cancer types is activated to provide important survival signals that prevent apoptosis, the above, unexpected findings pointed to the operation of a more complex process in inflammation-mediated hepatocarcinogenesis, in which mediators of the NFκB activation pathway have tumor suppressor roles (Luedde and Schwabe, 2011).

Because TAK1 and NEMO are subject to regulation by CYLD-mediated deubiquitination, we investigated the potential role of CYLD in liver cancer.

RESULTS

Spontaneous Hepatocyte Apoptosis and Liver Fibrosis in $CYLD^{L\Delta/\Delta}$ Mice

To study the role of CYLD in the liver, we generated mice carrying liver-specific homozygous deletion of *CYLD* exon 9 (designated $CYLD^{L\Delta/\Delta}$), by crossing mice carrying *CYLD* with floxed exon 9 (Trompouki et al., 2009) with *ALFP-Cre* transgenic mice (Kellendonk et al., 2000). Exon 9 deletion results in the expression of a deubiquitinase-deficient form of CYLD that mimics oncogenic mutations described in humans (Trompouki et al., 2009). Polymerase chain reaction (PCR) analysis of hepatocytes from newborn mice confirmed that excision of exon 9 was complete during embryonic life (data not shown). In adult stages, $CYLD^{L\Delta/\Delta}$ mice display hepatomegaly and perceptible stiffness (Figure 1A; Table S1 available online). Western blot analyses and immunostainings using an antibody recognizing the C-terminal epitope of CYLD revealed loss of detectable signals in all hepatocytes, but not in biliary epithelial cells and other smaller non-hepatocyte cells (Figures 1A and 1B), suggesting that *ALFP-Cre*-driven excision of *CYLD* exon 9 in embryonic life is hepatocyte-specific and occurs after hepatoblasts have differentiated into hepatocytes. Interestingly, CYLD exhibits a partially zonal expression pattern in wild-type livers, with higher levels of expression in periportal hepatocytes and reduced levels in hepatocytes surrounding the central veins (Figure 1B). Hematoxylin eosin staining of $CYLD^{L\Delta/\Delta}$ liver sections revealed disorganized regions around the portal veins containing cells with smaller nuclei as early as postnatal day 35 (P35). At later stages of postnatal development (P45 to P120), the number of these cells was dramatically increased, resulting in a staining pattern that highly resembles fibrotic livers (Figure 1C). Indeed, we could detect fibrillar collagen deposition by Sirius red staining initially around portal veins, which was gradually enhanced at later time points, resulting in a massively fibrotic liver at postnatal day 60 (P60) and postnatal day 120 (P120) (Figures 1D and 1E). This correlated with the appearance and expansion of activated hepatic stellate cells (HSCs) visualized by α smooth muscle actin (αSMA) staining (Figure S1A).

Liver damage and associated hepatocyte death is a prerequisite for stellate cell activation. In line with this, TUNEL assays detected substantial cell death around the portal veins of $CYLD^{L\Delta/\Delta}$ livers, as early as P25 (Figures 2A and 2B). The number of TUNEL positive apoptotic cells was greatly increased during the period between P25 and P120, which correlated with increasing levels of cleaved caspase 3 and parallel elevation of serum ALT levels (Figures 2A–2D). These results also indicate that apoptosis is the main pathway of cell death in $CYLD^{L\Delta/\Delta}$ livers. Supporting this notion, only a negligible increase in the levels of the necrosis marker RIP3 protein was detected in $CYLD^{L\Delta/\Delta}$ livers (Figure S1B).

To understand the mechanism by which CYLD inactivation leads to cell death, we first analyzed the activation of Jun N-terminal kinase (JNK), which is known to trigger apoptosis in several cell types when its activity is sustained for long periods of time (Kamata et al., 2005; Schwabe and Brenner, 2006). Spontaneous activation of JNK was observed in $CYLD^{L\Delta/\Delta}$ livers from P25 day onward (Figure 2E). The enhanced intensity of the phospho-JNK signal in western blots of extracts from P35, P45, and P60 $CYLD^{L\Delta/\Delta}$ livers correlated with an increased number of phospho-JNK positive hepatocytes detected by immunohistochemistry (Figure 2F). Double staining with HNF4 antibody revealed that more than 90% of p-JNK positive cells were hepatocytes at P25 and P35 days, while at later time points hepatocytes corresponded to about two-thirds of the pJNK positive cell population (Figure 2G). Importantly, phospho-JNK positive hepatocytes were initially observed only around portal veins, while at later time points, cells in the surrounding area toward the central veins also stained positively (Figure 2F). Activation of JNK was confirmed by a similar time-dependent induction of c-JUN phosphorylation (Figure 2H) and by the induction of expression of downstream target genes *DR5* and *PUMA* (Figure S2A).

Further evidence for the role of sustained JNK activation in hepatocyte death in $CYLD^{L\Delta/\Delta}$ livers was provided by experiments using the JNK inhibitor compound SP600125. Apoptosis and fibrosis were dramatically reduced in mice that were treated twice daily with SP600125 between P30 and P60 compared to those treated with vehicle only (Figures S2B–S2F). In addition, we could detect phosphorylated JNK in primary hepatocytes from $CYLD^{L\Delta/\Delta}$ livers, whose levels increased after treatment

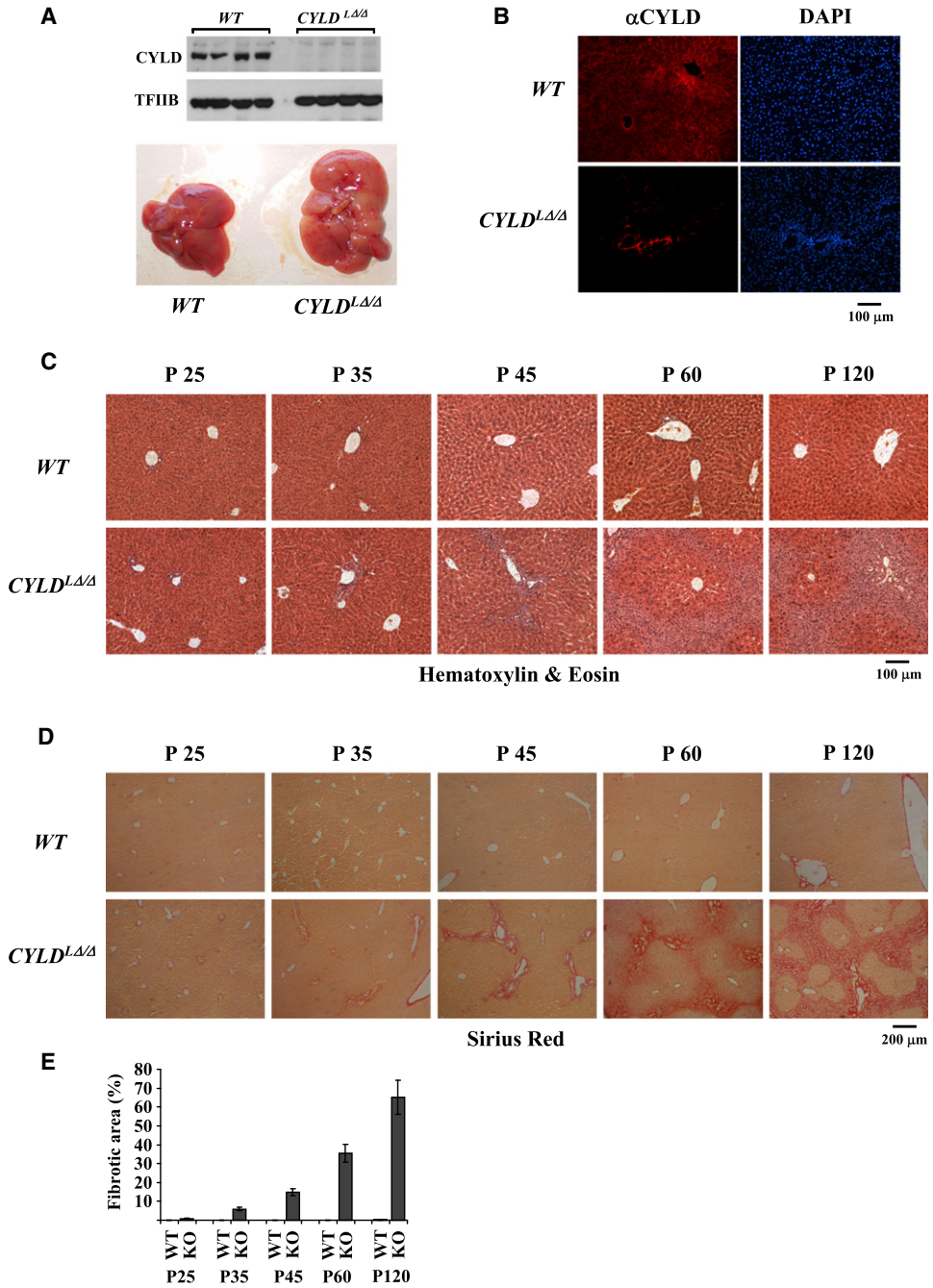

Figure 1. Loss of CYLD Causes Hepatomegaly, Histological Alterations, and Progressive Fibrosis in the Liver

(A) Western blot analysis of whole liver protein extracts from 45-day-old (P45) *CYLD*$^{lox/lox}$/*ALFP-Cre* (*CYLD*$^{L\Delta/\Delta}$) mice and control littermates (WT) using antibodies recognizing the C-terminal part of CYLD or TFIIB. Lower panel: Macroscopic appearance of P60 *CYLD*$^{L\Delta/\Delta}$ and WT livers.

(B) Representative immunohistological staining of liver sections from 45-day-old *CYLD*$^{L\Delta/\Delta}$ mice and control littermates (WT) with αCYLD antibody.

(C) Hematoxylin and Eosin staining of liver sections from postnatal 25-day-old (P25), 35-day-old (P35), 45-day-old (P45), 60-day-old (P60), and 120-day-old (P120) *CYLD*$^{L\Delta/\Delta}$ mice and control littermates (WT).

(D) Sirius Red staining of liver sections from mice indicated as in (C).

(E) Quantitation of Sirius red positive areas. Bars represent percentages of Sirius red positive areas compared to total areas and standard errors of the mean (SEM) from data obtained by examination of nine whole sections from three different animals.

See also Figure S1 and Table S1.

with TNFα (Figure S2G). In wild-type hepatocytes, TNFα-mediated JNK activation was transient but could be prolonged by priming with cycloheximide (CHX). In contrast, prolonged JNK activation without CHX was readily detected in *CYLD*$^{L\Delta/\Delta}$ hepatocytes (Figure S2I). The length of JNK activation correlated with the extent of cell death mediated by TNFα: significant

TNFα-induced cell death could be observed in $CYLD^{L\Delta/\Delta}$ hepatocytes, without concomitant CHX treatment, while in the case of wild-type cells, it was detected only after CHX priming (Figure S2H). Importantly, inhibition of JNK activation by SP600125 greatly prevented death in both cases (Figure S2H).

Collectively, the above results indicate that CYLD inactivation causes spontaneous hepatocyte death via prolonged activation of JNK. In turn, hepatocyte damage triggers the activation and proliferation of hepatic stellate cells, which produce ECM proteins generating progressively expanding fibrotic lesions.

Constitutive Hyperactivation of TAK1 in $CYLD^{L\Delta/\Delta}$ Mice

The mechanism of prolonged JNK activation-mediated apoptosis in our mouse model is likely to involve upstream signaling enzymes, which are direct enzymatic targets of CYLD. In agreement with this, western blot analysis using phospho-specific TAK1 antibodies detected spontaneous activation of TAK1 in $CYLD^{L\Delta/\Delta}$ livers and in primary hepatocyte extracts (Figures 3A and S3A). Phospho-TAK1 induction in $CYLD^{L\Delta/\Delta}$ livers positively correlated with increased K63-linked ubiquitination of endogenous TAK1 (Figure 3C). The amount of phosphorylated TAK1 was further elevated upon LPS treatment (Figure 3B). Importantly, high phospho-TAK1 levels were sustained for at least 2 hr following LPS treatment in $CYLD^{L\Delta/\Delta}$ livers, as opposed to wild-type livers in which TAK1 phosphorylation declined after 1 hr (Figure 3B).

To obtain direct evidence into the role of TAK1 hyperactivation in the phenotype of $CYLD^{L\Delta/\Delta}$ mice, we generated liver-specific $CYLD^{L\Delta/\Delta}/TAK1^{L\Delta/\Delta}$ double knockout mice. In agreement with previous reports (Bettermann et al., 2010; Inokuchi et al., 2010), $TAK1^{L\Delta/\Delta}$ mice developed early liver tumors as evidenced by macroscopically visible nodules in the liver, and, by the observation of cellular dysplasia, lost portal tracts and the appearance of cells with enlarged and hyperchromatic nuclei (Figures 3D and 3E). Serum ALT levels were dramatically induced, reaching levels that were four times higher than those detected in $CYLD^{L\Delta/\Delta}$ mice (Figure 3K). TAK1-deficient mice also displayed liver fibrosis and apoptosis, albeit at much lower levels compared to those observed in $CYLD^{L\Delta/\Delta}$ mice (Figures 3E–3I).

The phenotype of 2-month-old $CYLD^{L\Delta/\Delta}/TAK1^{L\Delta/\Delta}$ double knockout mice greatly differed from that observed in $CYLD^{L\Delta/\Delta}$ mice and very much resembled that of $TAK1^{L\Delta/\Delta}$ mice. Double knockout mice did not develop hepatomegaly, as was seen in $CYLD^{L\Delta/\Delta}$ mice. Instead, cancerous nodules were observed, as was seen in $TAK1^{L\Delta/\Delta}$ mice. Hepatic fibrosis and apoptosis and pJNK levels were dramatically reduced in double knockout mice while serum ALT levels were increased, reaching a level comparable to $TAK1^{L\Delta/\Delta}$ mice (Figures 3D–3K and Table S1). Importantly, the few apoptotic cells observed in different fields were scattered throughout the liver parenchyma in the $CYLD^{L\Delta/\Delta}/TAK1^{L\Delta/\Delta}$ double knockout mice as opposed to their periportal zonation in $CYLD^{L\Delta/\Delta}$ mice (Figures 3G and 2A). Likewise, the relatively minor fibrotic lesions in the $CYLD^{L\Delta/\Delta}/TAK1^{L\Delta/\Delta}$ double knockout mice appeared around both central and portal areas, a distribution that clearly differed from the strict periportal pattern observed in $CYLD^{L\Delta/\Delta}$ mice (Figure 3E). These quantitative and qualitative differences suggest that induction of cell death is achieved via different mechanisms in TAK1 and CYLD-deficient mice. Nevertheless, we can conclude that TAK1 activation is required for the initiation of periportal cell death and fibrosis in $CYLD^{L\Delta/\Delta}$ mice, as these early phenotypic changes were not observed in $CYLD^{L\Delta/\Delta}/TAK1^{L\Delta/\Delta}$ double knockout mice.

Constitutively active TAK1 can fully explain the observed long-term activation of JNK in $CYLD^{L\Delta/\Delta}$ hepatocytes, as it acts upstream of JNK. However, other mechanisms, including reactive oxygen species (ROS) accumulation, may also contribute to it (Kamata et al., 2005; He et al., 2010). To explore this possibility, ROS production was evaluated by staining liver sections with the H_2O_2-sensitive fluorescent dye CM-H_2DCFDA. As shown in Figure S3B, a few positive signals can be specifically detected in $CYLD^{L\Delta/\Delta}$ liver sections as early as P35, which greatly expand at P60 and 1 year of age. Similar to previous findings in IKKβ-deficient mice (He et al., 2010), ROS production resulted in the activation of STAT3 in $CYLD^{L\Delta/\Delta}$ mice (Figure S4A). No significant differences were detected in activated p38 levels, which also acts downstream of TAK1 (Figure S4B). Thus, we conclude that, apart from constitutively active TAK1, the accumulation of ROS, especially at later stages, can play a significant role in sustaining JNK activation and the consequent hepatocyte death.

Expansion of Cell Death in $CYLD^{L\Delta/\Delta}$ Livers Requires TNF Receptor Signaling

As described above, initially (at P25) only few apoptotic cells could be detected in the periportal region of $CYLD^{L\Delta/\Delta}$ livers, whose number gradually increased over time and expanded toward central veins. A possible explanation for this phenomenon could be that the initial, periportally restricted spontaneous hepatocyte injury could trigger inflammation and the consequent inflammation-mediated death receptor signaling may induce more widespread hepatocyte apoptosis. To explore this hypothesis, we first analyzed Kupffer cell activation using the F4/80 and CD68 macrophage markers. As shown in Figure 4A and Figure S4C, we could detect an increasing number of F4/80 and CD68 positive cells in $CYLD^{L\Delta/\Delta}$ livers from day P35 and onward. Using the CD45 marker, we also observed the appearance and expansion of other inflammatory cells in a similar time-dependent manner (Figure 4B). A parallel increase in hepatic *TNFα* mRNA levels was detected (Figure 4C). NFκB activation was evaluated by electrophoretic mobility shift assays and immunostaining. After LPS treatment, activated NFκB signal in $CYLD^{L\Delta/\Delta}$ livers occurred earlier than in wild-type livers, suggesting that loss of CYLD sensitizes hepatocytes to LPS-mediated NFκB activation (Figure 4D). TNFα-mediated activation of NFκB was more pronounced in $CYLD^{L\Delta/\Delta}$ primary hepatocytes, but unlike JNK activation, the induction of NFκB was transient, displaying a similar time-dependent decline in wild-type and CYLD-deficient cells (Figure S4D).

Unexpectedly, the earliest time point when activation of NFκB could be detected in vivo was only at P45 (Figure 4D). This coincides with the timing of first detection of elevated levels of hepatic *TNFα* mRNA (Figure 4C). Potential technical concerns in the sensitivity of the assay were eliminated by examining the expression of NFκB target cellular FLICE-like inhibitory protein

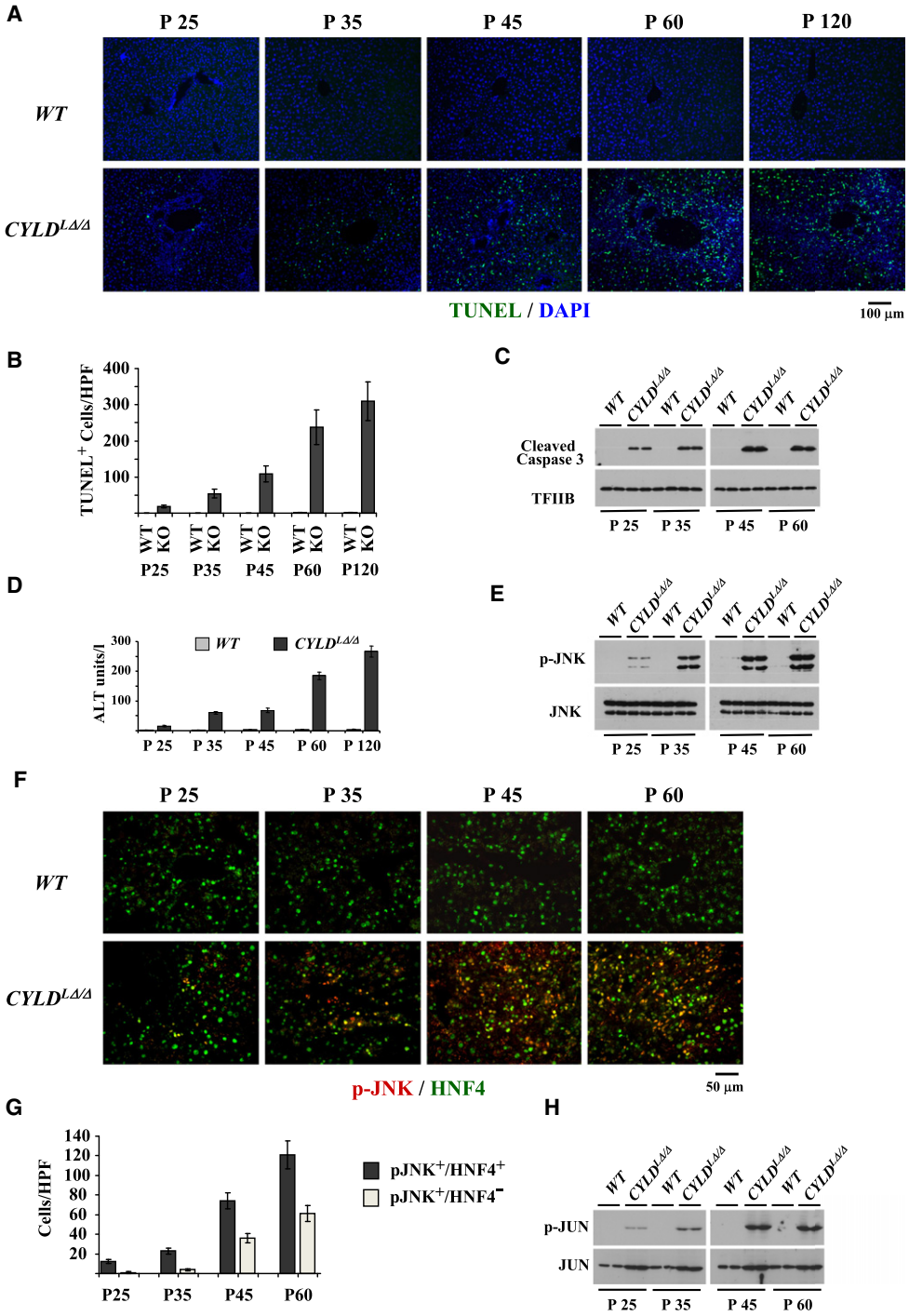

Figure 2. Liver-Specific Ablation of CYLD Leads to Spontaneous and Persistent Activation of JNK and Hepatocyte Apoptosis

(A) TUNEL staining of apoptotic cells in sections from livers of *CYLD*$^{L\Delta/\Delta}$ mice and control littermates (WT) between 25 and 120 days.

(B) Quantitation of TUNEL positive cells. Bars represent mean numbers of TUNEL positive cells per high power field (HPF) and SEM in 10 HPFs of three different animals.

(C) Western blot analysis of extracts from individual livers of 25- to 60-day-old *CYLD*$^{L\Delta/\Delta}$ mice and control littermates (WT) using an antibody specifically detecting cleaved caspase 3 (upper panel) or TFIIB (lower panel).

(D) Serum alanine aminotransferase levels (ALT) in 25- to 120-day-old *CYLD*$^{L\Delta/\Delta}$ mice and control littermates (WT). Bars represent mean values and SEM from samples of five individual mice.

(E) Western blot analysis of extracts from individual livers using antibody recognizing the Thr183/Tyr185-phosphorylated form of JNK (p-JNK) or total JNK (JNK).

(F) Immunohistological staining of liver sections from mice indicated as in (B) using phospho-JNK and HNF4 antibody.

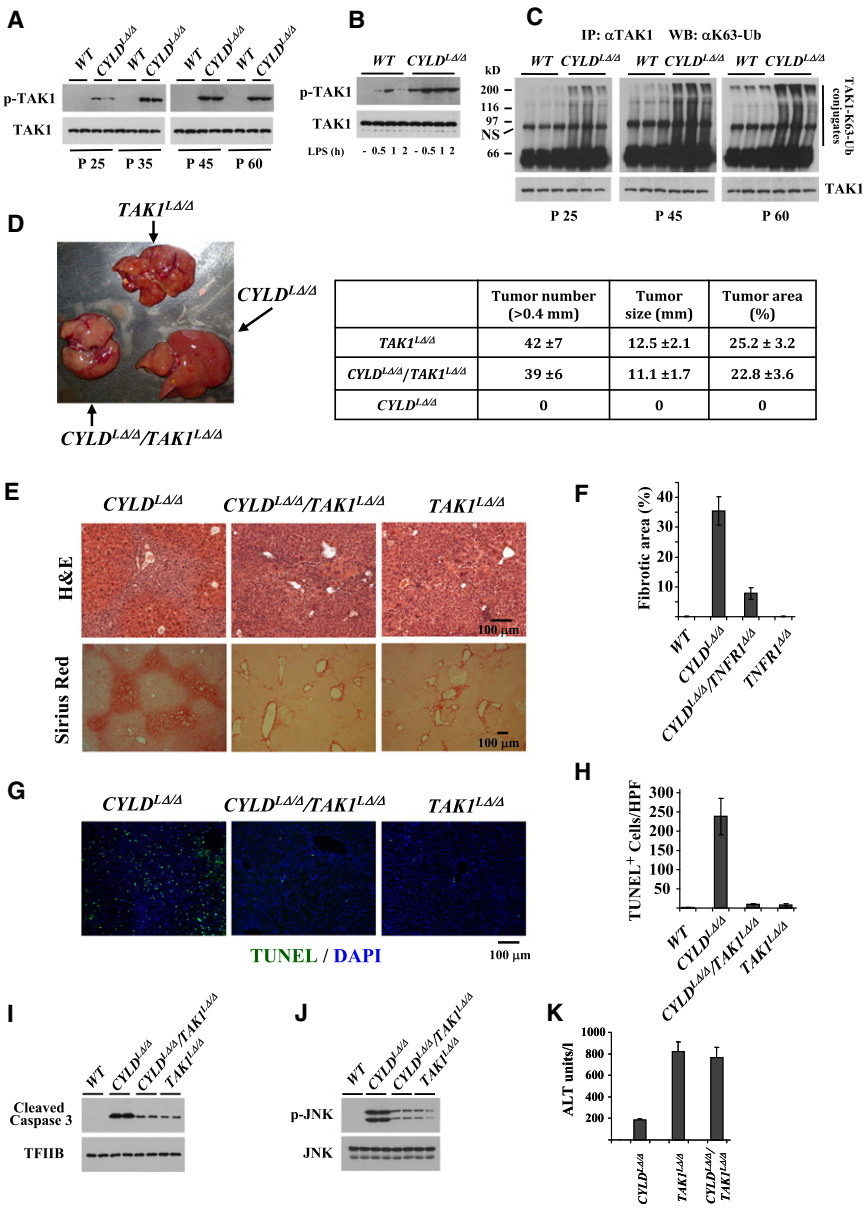

	Tumor number (>0.4 mm)	Tumor size (mm)	Tumor area (%)
TAK1$^{L\Delta/\Delta}$	42 ±7	12.5 ±2.1	25.2 ± 3.2
CYLD$^{L\Delta/\Delta}$/*TAK1*$^{L\Delta/\Delta}$	39 ±6	11.1 ±1.7	22.8 ±3.6
CYLD$^{L\Delta/\Delta}$	0	0	0

Figure 3. Spontaneous Activation of TAK1 Is Required for Apoptosis and Fibrosis in Liver-Specific CYLD-Deficient Mice

(A) Western blot analysis of extracts from individual livers of P25 to P60 *CYLD*$^{L\Delta/\Delta}$ mice and control littermates (WT) using an antibody specifically detecting the Thr184/187-phosphorylated form of TAK1 (p-TAK1) and total TAK1 (TAK1).

(B) Western blot analysis of extracts from the livers P60 *CYLD*$^{L\Delta/\Delta}$ mice and control littermates (WT) prepared at the indicated time points after intraperitoneal injection with 5 mg/kg LPS.

(C) Detection of K63-linked polyubiquitination of TAK1 in liver extracts from animals indicated as in (A) by immunoprecipitation with αTAK1 antibody followed by western blot analysis using αK63-Ub antibody. The amounts of total TAK1 in the immunoprecipitates were detected by western blot using αTAK1 antibody (bottom panel).

(D) Macroscopic appearance of 60-day-old *TAK1*$^{lox/lox}$/*ALFP-Cre* (*TAK1*$^{L\Delta/\Delta}$), *CYLD*$^{L\Delta/\Delta}$, and *CYLD*$^{lox/lox}$/*TAK1*$^{lox/lox}$/*ALFP-Cre* (*CYLD*$^{L\Delta/\Delta}$ / *TAK1*$^{L\Delta/\Delta}$) livers. The number of tumor foci, tumor sizes, and areas were evaluated in five mice at 2 months of age.

(E) Hematoxylin-eosin and Sirius red staining of liver sections from P60 *CYLD*$^{L\Delta/\Delta}$, *CYLD*$^{L\Delta/\Delta}$/*TAK1*$^{L\Delta/\Delta}$, and *TAK1*$^{L\Delta/\Delta}$ mice.

(F) Quantitation of Sirius red positive areas.

(G and H) TUNEL assays in liver sections and quantitations in P60 mice indicated as in (E).

(I) Western blot assay detecting cleaved caspase 3 in P60 mice indicated as in (E).

(J) Western blot assay detecting p-JNK in P60 mice indicated as in (E).

(K) Serum ALT levels in mice indicated as in (E). Bars represent mean values and SEM from samples of five individual mice.

See also Figure S3.

(cFLIP) and by immunohistochemical assays detecting the distribution of NFκB between the nucleus and the cytoplasm. Increased cFLIP protein levels were detected in P45 and P60 *CYLD*$^{L\Delta/\Delta}$ livers, but not at earlier time points (Figure S4E). Despite examining a large number of fields, we could not identify cells with nuclear NFκB staining at P25 and P35 (Figure 4E and data not shown). In contrast, our immunohistochemical assays indicate that the source of the observed NFκB DNA binding signal at P60 must be, at least in part, hepatocytes, as we detected nuclear localization of NFκB-p65 in several hepatocytes of P60 *CYLD*$^{L\Delta/\Delta}$ livers (Figure 4E).

Compelling evidence for the requirement of TNF receptor signaling in the expansion of hepatocyte apoptosis was provided by the data obtained with *CYLD*$^{L\Delta/\Delta}$/*TNFR1*$^{-/-}$ double knockout mice. Genetic ablation of *p55-TNFR1* in CYLD-deficient mice prevented the development of hepatomegaly (Figure 5A and Table S1). Sirius red and TUNEL staining was limited to the periportal area in 2-month-old mice, without expansion to the neighboring areas (Figures 5B–5E). In agreement with the reduced number of TUNEL positive cells, we detected smaller amounts of cleaved caspase 3 and serum alanine transaminase (ALT) levels in

(G) Quantitation of pJNK positive hepatocytes. Bars represent mean numbers per HPF and SEM of JNK positive hepatocytes (JNK+/HNF4+) and JNK positive non-hepatic cells (JNK+/HNF4-) in 10 HPFs of three different mice.

(H) Western blot analysis of extracts from individual livers using antibody recognizing Ser63-phosphorylated form of c-JUN (p-JUN) or total JUN (JUN).

See also Figure S2.

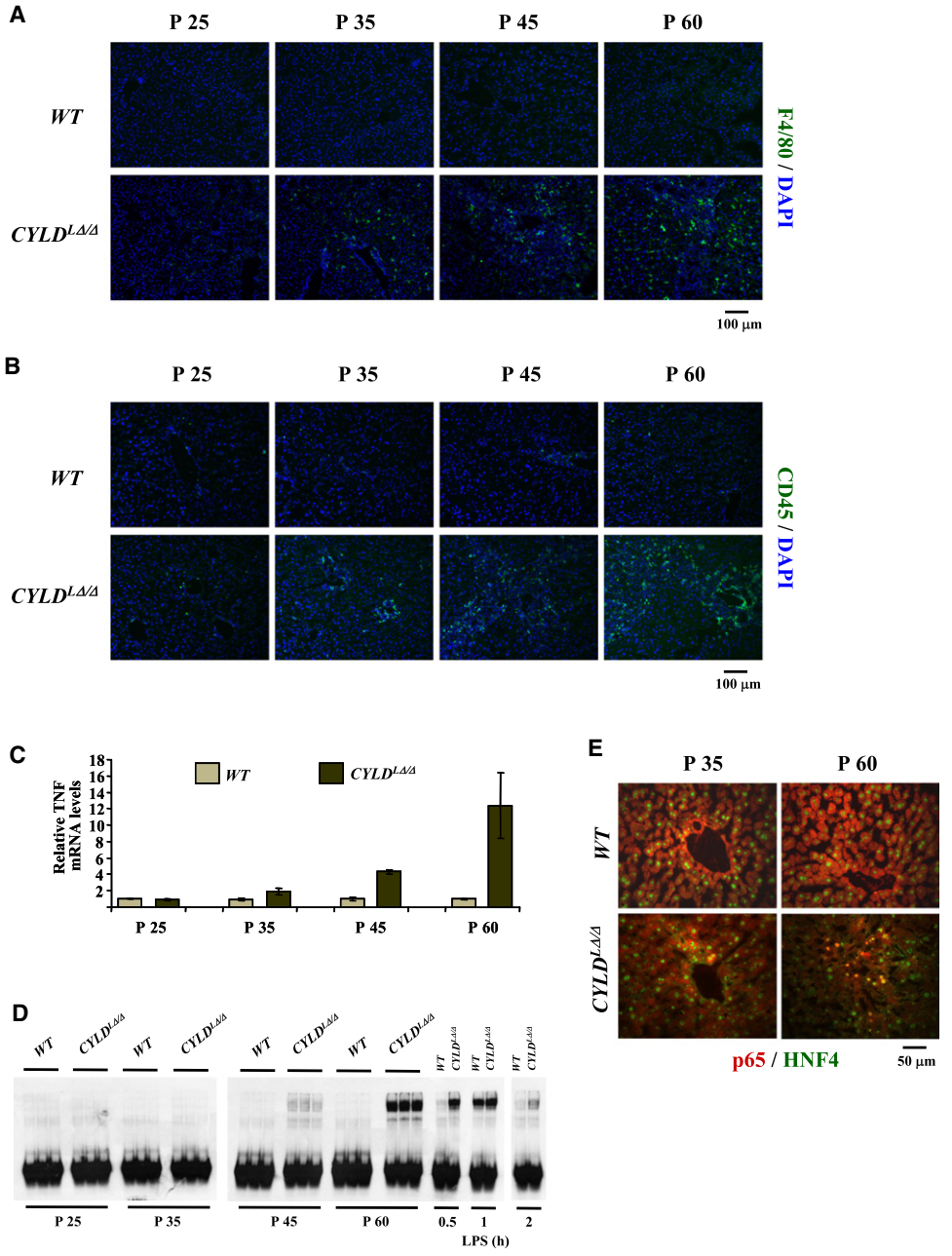

Figure 4. Spontaneous and Progressive Kupffer Cell Activation, Inflammatory Cell Infiltration, TNF Production, and NFκB Activation in the Livers of CYLD-Deficient Mice

(A and B) Immunohistological staining of liver sections from P25 to P60 *CYLD*$^{L\Delta/\Delta}$ mice and control littermates (WT) with F4/80 and CD45 antibody.

(C) *TNFα* mRNA levels from RT-qPCR assays in the livers of mice as indicated in (A). Bars represent mean values of TNFα mRNA levels normalized to glyceraldehyde-3-phosphate dehydrogenase (*GAPDH*) mRNA and SEM from samples of four individual mice.

(D) Electrophoretic mobility shift assays were performed using radioactive double stranded oligonucleotide containing NFκB binding site sequence and extracts from the livers of indicated mice. Where indicated, mice were injected intraperitoneally with 5 mg/kg LPS.

(E) Representative immunohistological staining detects cytoplasmic and nuclear NFκB-p65 in P35 and P60 *CYLD*$^{L\Delta/\Delta}$ mice and control littermate (WT).

See also Figure S4.

CYLD$^{L\Delta/\Delta}$/*TNFR1*$^{-/-}$ mice compared to *CYLD*$^{L\Delta/\Delta}$ mice (Figures 5F and 5G).

These data suggest that after the initial spontaneous apoptosis of periportal hepatocytes, inflammatory cells are recruited to the liver, in parallel with proliferation and activation of resident Kupffer cells. They produce inflammatory cytokines, such as TNFα, which, in turn, induce apoptosis in neighboring cells via the TNFR1-dependent signaling cascade.

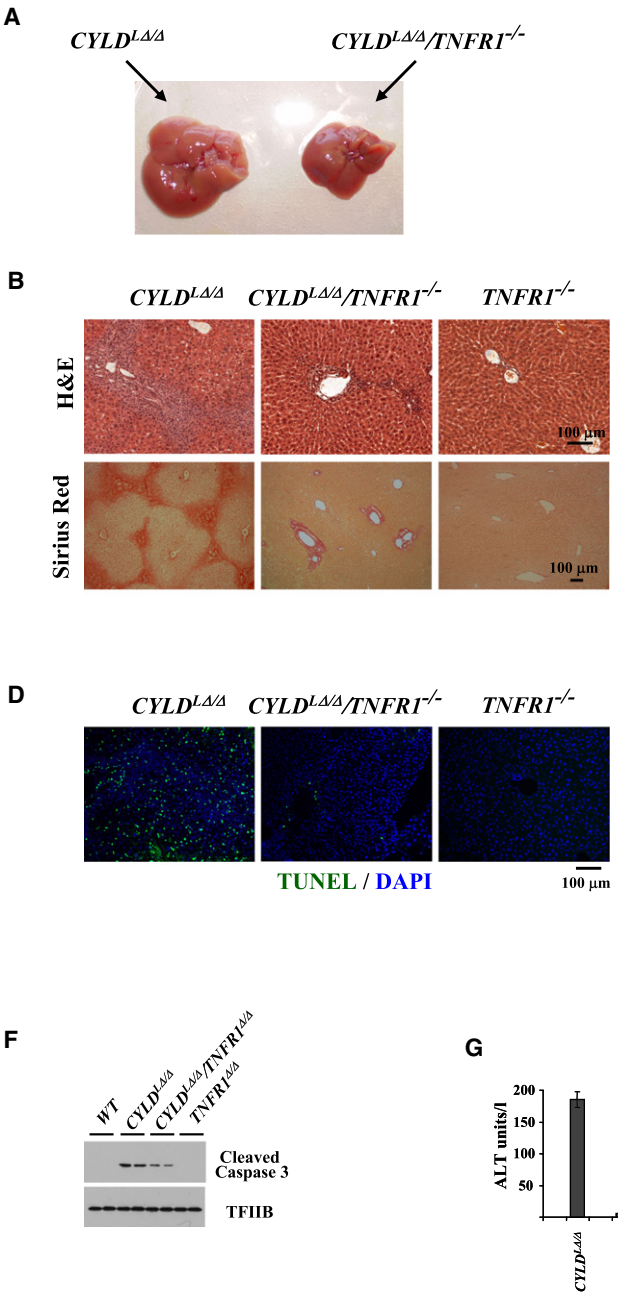

Figure 5. TNF Receptor 1 Is Required for the Expansion of Apoptosis and Fibrosis in Liver-Specific CYLD-Deficient Mice

(A) Macroscopic appearance of P60 $CYLD^{L\Delta/\Delta}$ and $CYLD^{L\Delta/\Delta}$ /$TNFR1^{-/-}$ livers.

(B) Hematoxylin-eosin and Sirius red staining of liver sections from P60 $CYLD^{L\Delta/\Delta}$, $CYLD^{L\Delta/\Delta}$/$TNFR1^{-/-}$, and $TNFR1^{-/-}$ livers mice.

(C) Quantitation of Sirius red positive areas.

(D and E) TUNEL assays and quantitation of P60 livers indicated as in (B).

(F) Western blot analysis of extracts from individual livers of P60 mice indicated as in (B) using an antibody specifically detecting cleaved caspase 3 (upper panel) or TFIIB (lower panel).

(G) Serum ALT levels in mice indicated as in (B). Bars represent mean values and SEM from samples of 5 individual mice.

Late Onset Development of Hepatocellular Carcinoma in $CYLD^{L\Delta/\Delta}$ Mice

Examination of 12-month-old $CYLD^{L\Delta/\Delta}$ livers revealed the presence of numerous cancerous foci of different sizes (Figure 6A). Microscopically, we could detect several histopathological features of hepatocellular carcinoma, including nuclear atypia, frequent pleomorphism, irregular trabeculae, obliteration of portal tracts, mitotic figures, and the presence of cells with increased eosinophilic inclusions or cytoplasmic clearance (Figure 6B).

Genome-wide comparative genomic hybridization (CGH) analysis revealed a large number of amplifications and deletions ranging from 0.62 MB to 14.8 MB in all chromosomes (Figure S5). Notably, several of the amplifications or deletions were detected in foci derived from different animals, pointing to the existence of common signatures generated by CYLD-dependent signals that affect chromosomal integrity. In addition, the expression of several known oncogenes and tumor suppressor genes was upregulated (38 genes) or downregulated (9 genes) in 1-year-old $CYLD^{L\Delta/\Delta}$ livers (Table S2).

Malignant tumor formation was further confirmed by the detection of proliferating cells using BrdU and Ki67 staining and by the detection of increased *Cyclin D1* expression in $CYLD^{L\Delta/\Delta}$ livers (Figures 6D and 7A). Excessive inflammation and liver damage in $CYLD^{L\Delta/\Delta}$ mice was also evident from the massive infiltration of CD45 positive cells and the highly elevated serum ALT levels (Figures 6C and 6D). Importantly, we observed positive staining and/or increased RNA levels of several oncofetal HCC marker genes, such as alpha-fetoprotein (*AFP*), *H19*, insulin-like growth factor 2 (*IGF2*), as well as hepatic stem cell marker genes like glypican 3 (*GPC-3*), *CD133*, or the oval cell-specific *A6* (Figures 6D, 7A, and 7B). Interestingly, we could detect activation of *NANOG*, *SOX2*, and *KLF4*, which are involved in the maintenance of pluripotency of embryonic stem cells (Figure 7C). Within the tumor area, about 25% of HNF4 positive cells stained positively for SOX2 and all SOX2 positive cells co-stained for HNF4 (Figure 7D).

The mRNA and protein levels of *β-catenin* were significantly increased in $CYLD^{L\Delta/\Delta}$ livers. However, the observed increase was due to the accumulation of non-hepatic cells with elevated *β-catenin* expression (Figure S6). Of note, in both wild-type and $CYLD^{L\Delta/\Delta}$ livers, we could detect only the membrane-associated form of the protein, which argues

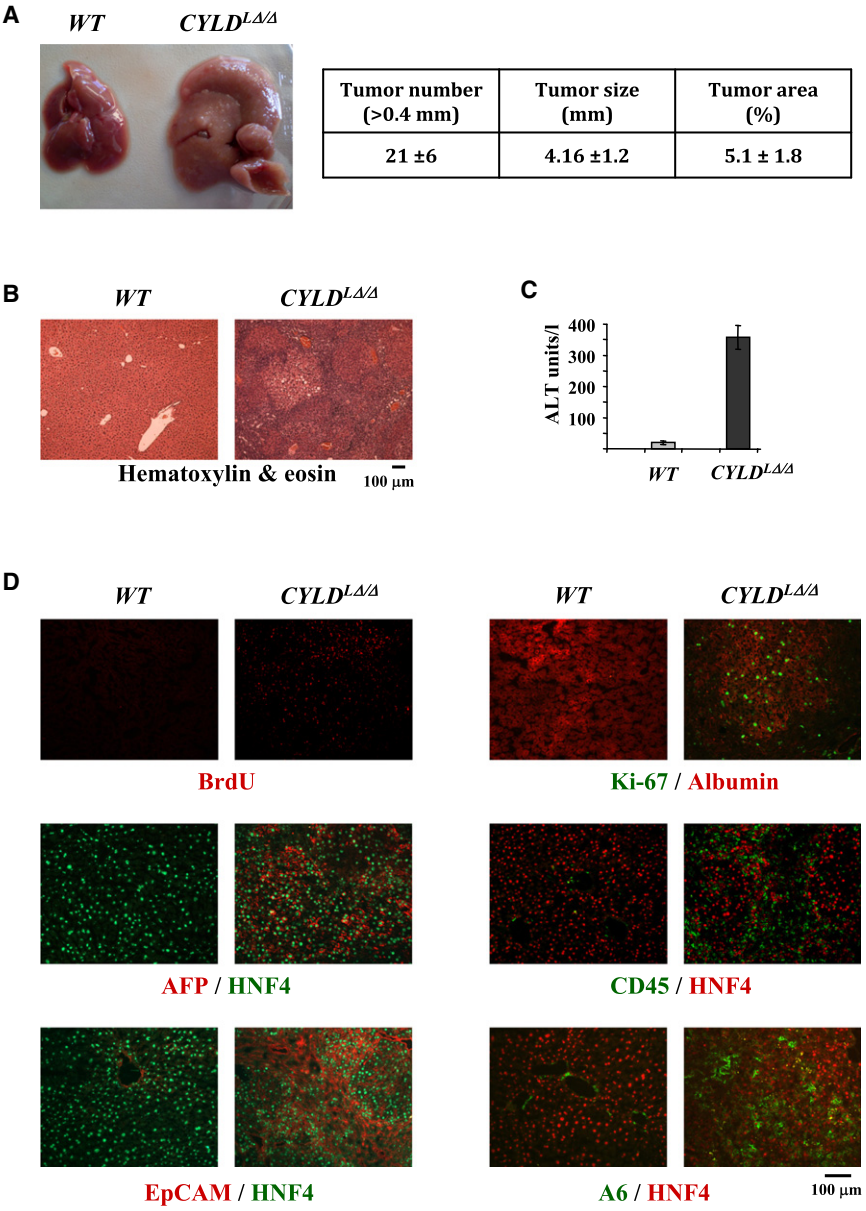

Figure 6. Spontaneous, Late-Onset Development of Hepatocellular Carcinoma in Liver-Specific CYLD-Deficient Mice

(A) Macroscopic appearance of 1-year-old $CYLD^{L\Delta/\Delta}$ mice and their control littermate (WT). The numbers of tumor foci, tumor sizes, and areas were evaluated in 11 mice at 1 year of age.

(B) Representative hematoxylin-eosin staining of liver sections of 1-year-old $CYLD^{L\Delta/\Delta}$ mice and their control littermate (WT).

(C) Serum ALT levels in 1-year-old mice. Bars represent mean values and SEM from samples of five individual mice.

(D) Representative immunohistochemical staining of liver sections of 1-year-old $CYLD^{L\Delta/\Delta}$ mice and control littermates (WT) with combinations of antibodies indicated at the bottom of the images. See also Figure S5.

against the involvement of Wnt signaling in the process of tumorigenesis.

The expression of other cancer marker genes, including connective tissue growth factor (*CTGF*) and *EpCAM*, was also increased in $CYLD^{L\Delta/\Delta}$ livers (Figures 6D and 7A). Counterstaining of the sections with the hepatocyte markers HNF4 or albumin showed that all of the AFP positive cells and a large number of Ki-67, EpCAM, or A6 positive cells are hepatocytes. Positive staining for EpCAM and A6, which besides cancerous hepatocytes also mark biliary epithelial cells in normal liver, was observed in a significant number of non-hepatic cells. These cells may correspond to proliferating cholangiocytes (Figure 6D). The observed mixed pattern of *EpCAM* and *A6* expression, together with the expression of oncofetal and stem cell marker genes, suggests that the tumors developing in $CYLD^{L\Delta/\Delta}$ livers resemble highly aggressive hepatocellular carcinoma, possibly combined with cholangiocarcinoma.

DISCUSSION

Previous studies have established that CYLD is a negative regulator of NFκB activation (Trompouki et al., 2003; Brummelkamp et al., 2003; Kovalenko et al., 2003). Because NFκB is a key regulator of cell survival and plays a protective role against programmed hepatocyte death (Ghosh and Karin, 2002; Pikarsky et al., 2004; Schwabe and Brenner, 2006), its inhibition was assumed to contribute to the known tumor suppressor function of CYLD, at least in some malignancies (Espinosa et al., 2010; Sun, 2010). Contrasting this view, the results of the present study demonstrate that loss of CYLD in hepatocytes causes spontaneous apoptosis. Initial hepatocyte death triggers inflammation, fibrosis, and late onset carcinogenesis, pointing to the crucial role of CYLD in the control of hepatocyte homeostasis. Phenotypic and molecular-level analyses of liver-specific CYLD-deficient mice revealed at least three temporally distinct events schematically presented in Figure 7E.

The first observable phenotypic change in $CYLD^{L\Delta/\Delta}$ livers is spontaneous apoptosis of periportal hepatocytes (Figure 7E, left panel). This coincides with spontaneous activation of TAK1 and JNK. The well-known proapototic function of sustained JNK activation (Kamata et al., 2005; Sakurai et al., 2006; Schwabe and Brenner, 2006; Hui et al., 2008) provides a mechanistic explanation for the observed occurrence of cell death. JNK is a downstream substrate of the TAK1-induced kinase cascade, suggesting that the initial triggering event of cell death must be the spontaneous hyperactivation of TAK1. In agreement with this, periportally restricted apoptosis was not observed in $CYLD^{L\Delta/\Delta}/TAK1^{L\Delta/\Delta}$ double knockout mice.

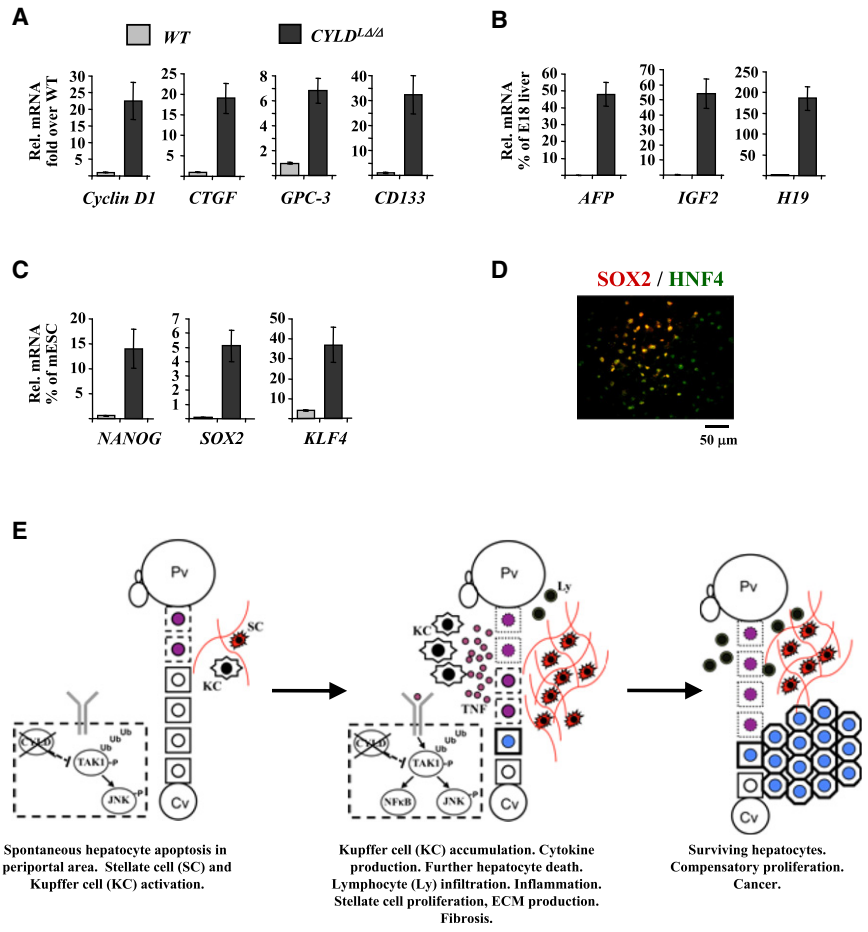

Figure 7. Hepatic Tumors Developed in *CYLD*$^{L\Delta/\Delta}$ Mice Express Oncofetal and Stem Cell-Specific Genes

(A–C) RT-qPCR assays in total liver RNA from 1-year-old *CYLD*$^{L\Delta/\Delta}$ mice and control littermates (WT) with primers amplifying the mRNAs of cancer and stem cell markers indicated at the bottom of the graphs. Bars represent mean mRNA levels normalized to GAPDH mRNA and SEM from samples of four individual mice. The data are presented either as a fold over wild-type values (A) for *Cyclin D1*, *CTGF*, *GPC-3*, and *CD133* mRNAs, or as percent of the values obtained with embryonic day 18.5 (E18) mouse livers (B) for *AFP*, *IGF2*, and *H19* mRNAs or as a percent of the values obtained with RNAs prepared from pluripotent mouse embryonic stem cells (C) *NANOG*, *SOX2*, and *KLF4* mRNAs.

(D) Representative immunohistochemical staining of liver sections of 1-year-old *CYLD*$^{L\Delta/\Delta}$ mice with SOX2 and HNF4 antibodies.

(E) Schematic presentation of the temporal order of molecular and phenotypic changes in liver-specific CYLD-deficient mice.

See also Table S2 and Figure S6.

How is TAK1 activated in the periportal hepatocytes of *CYLD*$^{L\Delta/\Delta}$ mice without external administration of signaling molecules? The most straightforward and simplest explanation is that the lack of CYLD-mediated cleavage of polyubiquitin chains increases K63-linked ubiquitination of TAK1, which stimulates TAK1 enzymatic activity independently of receptor signaling. An alternative, but conceptually related, mechanism is also suggested by our finding that CYLD-deficient hepatocytes, due to lack of deubiquitination-mediated control, are more sensitive to activate TAK1 in response to low amounts of LPS. Mice that are not kept under germ-free conditions are constantly challenged with small doses of lipopolysaccharide (LPS) produced by the intestinal bacterial flora, which can reach the liver via the portal tract and induce cytokine production by resident Kupffer cells (Enomoto et al., 2002). Thus, due to sensitization, hepatocytes in the periportal area of *CYLD*$^{L\Delta/\Delta}$ mice may respond to the locally available low amounts of LPS by activating TAK1 via death receptor signaling. Supporting this scenario is the time frame of apoptotic cell appearance: although CYLD is lost from hepatocytes before birth, apoptotic cells are first detected about 10 days after weaning (at P25), when the physiological bacterial flora of the gut is fully formed. Interestingly, CYLD is expressed at higher levels in periportal hepatocytes, compared to those in the pericentral area. We speculate that this partial zonal expression pattern may reflect an increased demand for CYLD-mediated control in the periportal area to protect hepatocytes from apoptosis induced by locally accumulating death-signaling molecules.

Following the initial apoptosis of periportal hepatocytes in *CYLD*$^{L\Delta/\Delta}$ mice, hepatic stellate cells and Kupffer cells are activated, leading to progressive fibrosis, inflammation, and TNFR1 signaling-dependent propagation of cell death into an expanded area of the liver (Figure 7E, middle panel). Dying hepatocytes release various mediators that induce transdifferentiation of hepatic stellate cells into myofibroblasts, which proliferate and produce a network of extracellular matrix, the hallmark of a fibrotic scar (Bataller and Brenner, 2005; Friedman, 2008). The resulting fibrosis acts as a precursor of cirrhosis during chronic liver damage-induced inflammation, in which excessive extracellular matrix deposition disrupts liver cytoarchitecture (Bataller and Brenner, 2005).

Similar to human fibrotic livers, hepatocyte death in *CYLD*$^{L\Delta/\Delta}$ mice is also associated with Kupffer cell activation and invasion of inflammatory cells parallel to stellate cell activation. Kupffer cells are resident macrophages in the liver and produce various inflammatory cytokines (Gao et al., 2008). In *CYLD*$^{L\Delta/\Delta}$ livers, the proliferation of Kupffer cells and the infiltration of other CD45 positive inflammatory cells correlated with the gradual increase of TNFα mRNA and phospho-JNK levels. This provides a mechanistic clue for the observed expansion of hepatocyte death toward the central vein areas, as locally elevated levels of TNFα could induce apoptosis in neighboring cells via the TNFR1-dependent signaling cascade. Evidence for this was provided by experiments in mice lacking both CYLD and p55-TNFR1. Apoptotic hepatocytes and fibrotic lesions in the double knockout mice were limited to the periportal areas even after

P60, suggesting that TNFR1 is required for the propagation of liver damage in $CYLD^{L\Delta/\Delta}$ mice.

We also noted that the expression of DR5 was highly increased in $CYLD^{L\Delta/\Delta}$ mice at P60, suggesting that signaling through DR5 may also contribute to the observed phenotype. However, such an effect should involve cooperation with TNFR-1, as the latter was absolutely required for the propagation and expansion of cell death in CYLD-deficient mice.

Of particular interest is the timing of NFκB activation in $CYLD^{L\Delta/\Delta}$ mice. As CYLD is known to act as a negative regulator of NFκB activation, it was surprising that we could not detect NFκB-p65 stimulation up until P45. The levels of activated NFκB-p65 peaked at P60, when massive cell death and inflammation was evident, but long after complete CYLD inactivation (embryonic life) or the first detection of apoptotic hepatocytes and TAK1 hyperactivation (P25). Although the mechanism behind this phenomenon is not understood, it is possible that the TAK1-NFκB activation cascade requires more robust signals that are available only at P45–P60 in $CYLD^{L\Delta/\Delta}$ livers. Thus, TAK1 activation does not always lead to NFκB induction. A similar lack of correlation between TAK1 and NFκB activation has also been observed in LPS-stimulated bone marrow-derived macrophages (Tseng et al., 2010). The observed preferential induction and chronic persistence of TAK1-JNK phosphorylation cascade over NFκB activation are in agreement with the observed cell death phenotype at the "early" stage. Induction of NFκB-p65 at later stages (at P60) cannot reverse cell death progression, suggesting that the dominance of the TAK1-JNK cascade, which persists for a long period of time, disrupts the balance between death signaling and compensatory survival pathways.

Loss of CYLD has been described in human hepatocellular carcinomas (Hellerbrand et al., 2007). The large majority of hepatocellular carcinomas are detected in patients with hepatic fibrosis or cirrhosis (Okuda, 2000). They develop in a setting of chronic hepatocyte injury and inflammation, similar to that observed in $CYLD^{L\Delta/\Delta}$ mice. In accordance with the above, we found that $CYLD^{L\Delta/\Delta}$ mice spontaneously developed hepatocellular carcinoma at the age of 12 months, pointing to a potential causative and mechanistic relationship between CYLD expression and the development of HCC. The preceding massive cell death and the late appearance of carcinoma in $CYLD^{L\Delta/\Delta}$ mice suggests that, similar to other HCC models generated by genetic ablation of NFκB regulators (Maeda et al., 2005; Luedde et al., 2007; Inokuchi et al., 2010; Bettermann et al., 2010), the mechanism of carcinogenesis involves compensatory cell proliferation (Figure 7E, right panel). Of interest is that the hepatocellular carcinoma in $CYLD^{L\Delta/\Delta}$ mice associates with the reactivation of oncofetal hepatic genes (*AFP*, *H19*, *IGF2*), with the expression of cancer stem cell (CSC) related genes (*GPC-3*, *CD133*), and with genes involved in maintenance of embryonic stem cells (*NANOG*, *SOX2*, *KLF4*). Activation of these latter genes has been implicated in highly aggressive epithelial tumors, with very poor prognosis (Ben-Porath et al., 2008). The above features demonstrate that tumors developing in $CYLD^{L\Delta/\Delta}$ livers highly resemble human hepatocellular carcinomas, whose expression profiles are enriched in stem cell traits (Marquardt et al., 2011). The activation of the oncofetal and "stem cell signature" genes may arise from the high degree of dedifferentiation of hepatocytes that enter the cell cycle via G0-G1 transition or from the proliferation of resident hepatic "stem cells," or both. The available data do not allow discrimination between these possibilities.

Compensatory cell growth could be initiated by ROS accumulation-mediated activation of the oncogenic transcription factor STAT3 (He et al., 2010). The high levels of STAT3 activation in $CYLD^{L\Delta/\Delta}$ mice from P60 and onward and the correlation of STAT3 activation with the levels of ROS accumulation provide a strong indication for its involvement in the process.

Both NEMO and TAK1 are subject to negative regulation by CYLD-mediated deubiquitination (Kovalenko et al., 2003; Reiley et al., 2007). Thus, it was surprising to see that several of the phenotypic characteristics $CYLD^{L\Delta/\Delta}$ mice resemble those reported in liver-specific NEMO and TAK1-deficient mice (Luedde et al., 2007; Inokuchi et al., 2010; Bettermann et al., 2010). The similar phenotypic features include: hepatocyte death, fibrosis, inflammation and cancer. The similarities between $CYLD^{L\Delta/\Delta}$ and $TAK1^{L\Delta/\Delta}$ mice are of particular concern, since TAK1 hyperactivation represents the earliest triggering event in the pathogenesis of liver damage observed in the $CYLD^{L\Delta/\Delta}$ mice. While our analysis of $TAK1^{L\Delta/\Delta}$ mice confirmed the findings of previous reports, it also revealed significant differences between $CYLD^{L\Delta/\Delta}$ and $TAK1^{L\Delta/\Delta}$ mice in terms of timing, localization, and the severity of cell death, fibrosis, and cancer phenotypes. $TAK1^{L\Delta/\Delta}$ mice, generated by crossing $TAK1^{lox}$ with *ALFP-Cre* (this study and Bettermann et al., 2010), developed full-blown HCC at 1.5 months of age, as opposed to $CYLD^{L\Delta/\Delta}$ mice, which develop cancer at 10–12 months of age. In contrast to the massive hepatocyte death and liver fibrosis of $CYLD^{L\Delta/\Delta}$ mice, TAK1-deficient livers display only a few TUNEL positive cells and much milder fibrotic lesions. An additional significant difference between $CYLD^{L\Delta/\Delta}$ and $TAK1^{L\Delta/\Delta}$ mice is the different local distribution of apoptotic hepatocytes and fibrotic lesions. Hepatocyte death and fibrosis are initially limited and later expand to an extended periportal zone in $CYLD^{L\Delta/\Delta}$ mice, while in TAK1-deficient mice, the small number of apoptotic cells and milder fibrotic lesions are uniformly distributed between central vein and portal vein areas.

Despite these qualitative and quantitative differences, the end result of both constitutive activation or inactivation of TAK1 is spontaneously developing inflammation and cancer. Thus, either aberrant increase or decrease of TAK1 activity is detrimental to hepatocyte function. Our results highlight the role of CYLD in keeping TAK1 activity in equilibrium, protecting the liver from spontaneous damage. Therefore, we propose that CYLD acts as a master regulator of TAK1-induced signaling cascades and plays a critical role in the maintenance of physiological liver homeostasis.

EXPERIMENTAL PROCEDURES

Animal Models

$CYLD^{lox}$ mice carrying floxed exon 9 alleles of *CYLD* have been described previously (Trompouki et al., 2009). To obtain liver-specific inactivation of *CYLD,* we crossed $CYLD^{lox}$ mice with *ALFP-Cre* transgenic mice (Kellendonk et al., 2000). $CYLD^{lox}$ littermates without *Cre* transgene were used as wild-type controls. For the generation of conditional TAK1-deficient mice, we crossed mice containing floxed TAK1 exon 2 allele (Eftychi et al.,

2012) with *ALFP-Cre* transgenic mice. *TNFR1*$^{-/-}$ mice have been described previously (Rothe et al., 1993). All animals were in C57Bl6 background. Mice were maintained in grouped cages in a temperature-controlled, specific-pathogen-free facility on a 12-hr light/dark cycle and fed by a standard chow diet (Altromin 1324; 19% protein, 5% fat) and water ad libitum. All animal experiments were approved by the Prefecture of Attica and were performed in accordance with the respective national and European Union regulations.

Histological Analysis

Histological assays were performed in paraffin-embedded or frozen tissue sections as described previously (Boulias et al., 2005; Kyrmizi et al., 2006). Briefly, livers were dissected, fixed in 4% paraformaldehyde, and embedded in paraffin. Liver sections (5–6 μm thick) were boiled in 10 mM Na-citrate for 20 min and, after washings with PBS, were blocked with normal goat serum in PBS and used for staining with αSMA antibody. For immunohistochemistry with all of the other antibodies, cryosections were used. Freshly isolated liver tissues were embedded in optimal cutting temperature (OCT) embedding medium without fixation and samples were frozen in liquid nitrogen. Frozen sections were air-dried before fixation in 4% formaldehyde for 15 min at room temperature. Blocking was performed in 1% BSA/0,1% Triton X-100 for 1 hr and then incubated with primary antibodies at room temperature for 2 hr or at 4°C overnight. After incubation with AlexaFluor 568, 555, or 488 (Molecular Probes) secondary antibodies for 1 hr at room temperature and counterstaining with DAPI, fluorescence images were observed using a Zeiss Axioscope 2 Plus microscope. Paraffin-embedded tissue sections were used for staining with 0.1% Sirius red dissolved in saturated picric acid or with hematoxylin and eosin (H&E). Sirius-red positive areas were quantitated using NIH Image-J software. TUNEL assays were performed using the Fluorescein cell death detection kit (Roche). To detect proliferating cells, mice were injected intraperitonelly with 1 mg/kg 5′-Bromo-2′-deoxyuridine (Sigma) twice, in 12-hr intervals. Incorporated BrdU was detected in cryosections using mouse monoclonal αBrdU antibody (Sigma).

Accumulation of reactive oxygen species (ROS) was measured by staining frozen liver sections with 2 μM of 5-(and-6)-chloromethyl-2′,7′-dichlorodihydrofluorescein diacetate, acetyl ester (CM-H_2DCFDA) for 30 min at 37°C. Cell survival in primary hepatocyte cultures was evaluated by MTT assays using 3-(4,5-dimethylthiazol-2-yl)-2,5-diphenyltetrazolium bromide, as described previously (Kontaki and Talianidis, 2010).

Biochemical Analysis

Blood was collected and centrifuged at 1000 g for 10 min. Freshly isolated supernatant plasma fractions were used for measuring alanine aminotransferase (ALT) activity with the Dyasis assay kit.

Preparation of nuclear and whole cell extracts, immunoprecipitations, and western blot assays were performed as described (Tatarakis et al., 2008; Martinez-Jimenez et al., 2010; Kontaki and Talianidis, 2010). For electrophoretic mobility shift assays, double-stranded oligonucleotide was radiolabeled by filling in with Klenow enzyme in the presence of α^{32}P-dCTP. The oligonucleotide used represents an NFκB consensus sequence: sense: 5′-GGG TTG AGG GGA CTT TCC CAG G; antisense: 5′-GGG CCT GGG AAA CTC CCC TCA A. Binding reactions were performed in 15 μl volume containing 20 mM HEPES pH 7.9, 50 mM KCl, 2 mM $MgCl_2$, 4 mM spermidine, 0.02 mM Zn-acetate, 0.1 μg/ml bovine serum albumin, 10% glycerol, 0.5 mM dithiotreitol, 2 μg poly (dI-dC), and 5 μg nuclear extracts. After incubation in ice for 30 min, the protein/DNA complexes were resolved in 5% native polyacrylamide gels and visualized by autoradiography.

RNA Analysis

Total RNA was prepared by the Trizol extraction. After digestion with DNase I, 1 μg of total RNA was used for first strand cDNA synthesis using MMLV reverse transcriptase. Quantitative PCR analyses were carried out in CHROMO4 Real time PCR detection system by using SYBR Green reagent, as described before (Kyrmizi et al., 2006). The nucleotide sequences of primer sets are shown in Supplementary Information. For global gene expression, profiling total RNAs from the whole livers of 1-year-old *CYLD*$^{L\Delta/\Delta}$ mice were analyzed using Affimetrix GeneChIP Exon 1.0 ST Arrays, as described previously (Tatarakis et al., 2008).

ACCESSION NUMBERS

Expression profiling and αCGH data were deposited to ArrayExpress under accession numbers E-MEXP-3478 and E-MTAB-905, respectively.

SUPPLEMENTAL INFORMATION

Supplemental Information includes six figures, two tables, and Supplemental Experimental Procedures and can be found with this article online at doi:10.1016/j.ccr.2012.04.026.

ACKNOWLEDGMENTS

We thank V. Harokopos, S. Kotschote, V. Factor, P. Hatzis, and the Graduate Program MBHD at the University of Crete, Medical School. This work was supported by grants from EU (HEALTH-F5-2009-241783), AICR (09-0586), and GSRT (09SYN-13-901, Thalis656).

Received: June 27, 2011
Revised: January 12, 2012
Accepted: April 2, 2012
Published: June 11, 2012

REFERENCES

Annunziata, C.M., Davis, R.E., Demchenko, Y., Bellamy, W., Gabrea, A., Zhan, F., Lenz, G., Hanamura, I., Wright, G., Xiao, W., et al. (2007). Frequent engagement of the classical and alternative NF-kappaB pathways by diverse genetic abnormalities in multiple myeloma. Cancer Cell *12*, 115–130.

Bataller, R., and Brenner, D.A. (2005). Liver fibrosis. J. Clin. Invest. *115*, 209–218.

Ben-Porath, I., Thomson, M.W., Carey, V.J., Ge, R., Bell, G.W., Regev, A., and Weinberg, R.A. (2008). An embryonic stem cell-like gene expression signature in poorly differentiated aggressive human tumors. Nat. Genet. *40*, 499–507.

Bettermann, K., Vucur, M., Haybaeck, J., Koppe, C., Janssen, J., Heymann, F., Weber, A., Weiskirchen, R., Liedtke, C., Gassler, N., et al. (2010). TAK1 suppresses a NEMO-dependent but NF-kappaB-independent pathway to liver cancer. Cancer Cell *17*, 481–496.

Bignell, G.R., Warren, W., Seal, S., Takahashi, M., Rapley, E., Barfoot, R., Green, H., Brown, C., Biggs, P.J., Lakhani, S.R., et al. (2000). Identification of the familial cylindromatosis tumour-suppressor gene. Nat. Genet. *25*, 160–165.

Boulias, K., Katrakili, N., Bamberg, K., Underhill, P., Greenfield, A., and Talianidis, I. (2005). Regulation of hepatic metabolic pathways by the orphan nuclear receptor SHP. EMBO J. *24*, 2624–2633.

Brummelkamp, T.R., Nijman, S.M., Dirac, A.M., and Bernards, R. (2003). Loss of the cylindromatosis tumour suppressor inhibits apoptosis by activating NF-kappaB. Nature *424*, 797–801.

Chen, Z.J. (2005). Ubiquitin signalling in the NF-kappaB pathway. Nat. Cell Biol. *7*, 758–765.

Eftychi, C., Karagianni, N., Alexiou, M., Apostolaki, M., and Kollias, G. (2012). Myeloid TAKL acts as a negative regulator of the LPS response and mediates resistance to endotoxemia. PLoS ONE *7*, e31550.

Enomoto, N., Takei, Y., Hirose, M., Ikejima, K., Miwa, H., Kitamura, T., and Sato, N. (2002). Thalidomide prevents alcoholic liver injury in rats through suppression of Kupffer cell sensitization and TNF-alpha production. Gastroenterology *123*, 291–300.

Espinosa, L., Cathelin, S., D'Altri, T., Trimarchi, T., Statnikov, A., Guiu, J., Rodilla, V., Inglés-Esteve, J., Nomdedeu, J., Bellosillo, B., et al. (2010). The Notch/Hes1 pathway sustains NF-κB activation through CYLD repression in T cell leukemia. Cancer Cell *18*, 268–281.

Friedman, S.L. (2008). Mechanisms of hepatic fibrogenesis. Gastroenterology *134*, 1655–1669.

Gao, B., Jeong, W.I., and Tian, Z. (2008). Liver: An organ with predominant innate immunity. Hepatology *47*, 729–736.

Ghosh, S., and Karin, M. (2002). Missing pieces in the NF-kappaB puzzle. Cell Suppl. *109*, S81–S96.

He, G., Yu, G.Y., Temkin, V., Ogata, H., Kuntzen, C., Sakurai, T., Sieghart, W., Peck-Radosavljevic, M., Leffert, H.L., and Karin, M. (2010). Hepatocyte IKKbeta/NF-kappaB inhibits tumor promotion and progression by preventing oxidative stress-driven STAT3 activation. Cancer Cell *17*, 286–297.

Hellerbrand, C., Bumes, E., Bataille, F., Dietmaier, W., Massoumi, R., and Bosserhoff, A.K. (2007). Reduced expression of CYLD in human colon and hepatocellular carcinomas. Carcinogenesis *28*, 21–27.

Hui, L., Zatloukal, K., Scheuch, H., Stepniak, E., and Wagner, E.F. (2008). Proliferation of human HCC cells and chemically induced mouse liver cancers requires JNK1-dependent p21 downregulation. J. Clin. Invest. *118*, 3943–3953.

Inokuchi, S., Aoyama, T., Miura, K., Osterreicher, C.H., Kodama, Y., Miyai, K., Akira, S., Brenner, D.A., and Seki, E. (2010). Disruption of TAK1 in hepatocytes causes hepatic injury, inflammation, fibrosis, and carcinogenesis. Proc. Natl. Acad. Sci. USA *107*, 844–849.

Kamata, H., Honda, S., Maeda, S., Chang, L., Hirata, H., and Karin, M. (2005). Reactive oxygen species promote TNFalpha-induced death and sustained JNK activation by inhibiting MAP kinase phosphatases. Cell *120*, 649–661.

Keats, J.J., Fonseca, R., Chesi, M., Schop, R., Baker, A., Chng, W.J., Van Wier, S., Tiedemann, R., Shi, C.X., Sebag, M., et al. (2007). Promiscuous mutations activate the noncanonical NF-kappaB pathway in multiple myeloma. Cancer Cell *12*, 131–144.

Kellendonk, C., Opherk, C., Anlag, K., Schütz, G., and Tronche, F. (2000). Hepatocyte-specific expression of Cre recombinase. Genesis *26*, 151–153.

Kontaki, H., and Talianidis, I. (2010). Lysine methylation regulates E2F1-induced cell death. Mol. Cell *39*, 152–160.

Kovalenko, A., Chable-Bessia, C., Cantarella, G., Israël, A., Wallach, D., and Courtois, G. (2003). The tumour suppressor CYLD negatively regulates NF-kappaB signalling by deubiquitination. Nature *424*, 801–805.

Kyrmizi, I., Hatzis, P., Katrakili, N., Tronche, F., Gonzalez, F.J., and Talianidis, I. (2006). Plasticity and expanding complexity of the hepatic transcription factor network during liver development. Genes Dev. *20*, 2293–2305.

Luedde, T., Beraza, N., Kotsikoris, V., van Loo, G., Nenci, A., De Vos, R., Roskams, T., Trautwein, C., and Pasparakis, M. (2007). Deletion of NEMO/IKKgamma in liver parenchymal cells causes steatohepatitis and hepatocellular carcinoma. Cancer Cell *11*, 119–132.

Luedde, T., and Schwabe, R.F. (2011). NF-κB in the liver—linking injury, fibrosis and hepatocellular carcinoma. Nat Rev Gastroenterol Hepatol *8*, 108–118.

Maeda, S., Kamata, H., Luo, J.L., Leffert, H., and Karin, M. (2005). IKKbeta couples hepatocyte death to cytokine-driven compensatory proliferation that promotes chemical hepatocarcinogenesis. Cell *121*, 977–990.

Marquardt, J.U., Raggi, C., Andersen, J.B., Seo, D., Avital, I., Geller, D., Lee, Y.H., Kitade, M., Holczbauer, A., Gillen, M.C., et al. (2011). Human hepatic cancer stem cells are characterized by common stemness traits and diverse oncogenic pathways. Hepatology *54*, 1031–1042. 10.1002/hep.24454.

Martinez-Jimenez, C.P., Kyrmizi, I., Cardot, P., Gonzalez, F.J., and Talianidis, I. (2010). Hepatocyte nuclear factor 4alpha coordinates a transcription factor network regulating hepatic fatty acid metabolism. Mol. Cell. Biol. *30*, 565–577.

Okuda, K. (2000). Hepatocellular carcinoma. J. Hepatol. *32* (1, Suppl), 225–237.

Pikarsky, E., Porat, R.M., Stein, I., Abramovitch, R., Amit, S., Kasem, S., Gutkovich-Pyest, E., Urieli-Shoval, S., Galun, E., and Ben-Neriah, Y. (2004). NF-kappaB functions as a tumour promoter in inflammation-associated cancer. Nature *431*, 461–466.

Reiley, W., Zhang, M., Wu, X., Granger, E., and Sun, S.C. (2005). Regulation of the deubiquitinating enzyme CYLD by IkappaB kinase gamma-dependent phosphorylation. Mol. Cell. Biol. *25*, 3886–3895.

Reiley, W.W., Jin, W., Lee, A.J., Wright, A., Wu, X., Tewalt, E.F., Leonard, T.O., Norbury, C.C., Fitzpatrick, L., Zhang, M., and Sun, S.C. (2007). Deubiquitinating enzyme CYLD negatively regulates the ubiquitin-dependent kinase Tak1 and prevents abnormal T cell responses. J. Exp. Med. *204*, 1475–1485.

Rincón, M., and Davis, R.J. (2009). Regulation of the immune response by stress-activated protein kinases. Immunol. Rev. *228*, 212–224.

Rothe, J., Lesslauer, W., Lötscher, H., Lang, Y., Koebel, P., Köntgen, F., Althage, A., Zinkernagel, R., Steinmetz, M., and Bluethmann, H. (1993). Mice lacking the tumour necrosis factor receptor 1 are resistant to TNF-mediated toxicity but highly susceptible to infection by Listeria monocytogenes. Nature *364*, 798–802.

Sakurai, T., Maeda, S., Chang, L., and Karin, M. (2006). Loss of hepatic NF-kappa B activity enhances chemical hepatocarcinogenesis through sustained c-Jun N-terminal kinase 1 activation. Proc. Natl. Acad. Sci. USA *103*, 10544–10551.

Schwabe, R.F., and Brenner, D.A. (2006). Mechanisms of Liver Injury. I. TNF-alpha-induced liver injury: role of IKK, JNK, and ROS pathways. Am. J. Physiol. Gastrointest. Liver Physiol. *290*, G583–G589.

Sun, S.C. (2008). Deubiquitylation and regulation of the immune response. Nat. Rev. Immunol. *8*, 501–511.

Sun, S.C. (2010). CYLD: a tumor suppressor deubiquitinase regulating NF-kappaB activation and diverse biological processes. Cell Death Differ. *17*, 25–34.

Tatarakis, A., Margaritis, T., Martinez-Jimenez, C.P., Kouskouti, A., Mohan, W.S., 2nd, Haroniti, A., Kafetzopoulos, D., Tora, L., and Talianidis, I. (2008). Dominant and redundant functions of TFIID involved in the regulation of hepatic genes. Mol. Cell *31*, 531–543.

Trompouki, E., Hatzivassiliou, E., Tsichritzis, T., Farmer, H., Ashworth, A., and Mosialos, G. (2003). CYLD is a deubiquitinating enzyme that negatively regulates NF-kappaB activation by TNFR family members. Nature *424*, 793–796.

Trompouki, E., Tsagaratou, A., Kosmidis, S.K., Dollé, P., Qian, J., Kontoyiannis, D.L., Cardoso, W.V., and Mosialos, G. (2009). Truncation of the catalytic domain of the cylindromatosis tumor suppressor impairs lung maturation. Neoplasia *11*, 469–476.

Tseng, P.H., Matsuzawa, A., Zhang, W., Mino, T., Vignali, D.A., and Karin, M. (2010). Different modes of ubiquitination of the adaptor TRAF3 selectively activate the expression of type I interferons and proinflammatory cytokines. Nat. Immunol. *11*, 70–75.

Vallabhapurapu, S., and Karin, M. (2009). Regulation and function of NF-kappaB transcription factors in the immune system. Annu. Rev. Immunol. *27*, 693–733.

Wright, A., Reiley, W.W., Chang, M., Jin, W., Lee, A.J., Zhang, M., and Sun, S.C. (2007). Regulation of early wave of germ cell apoptosis and spermatogenesis by deubiquitinating enzyme CYLD. Dev. Cell *13*, 705–716.

Yoshida, H., Jono, H., Kai, H., and Li, J.D. (2005). The tumor suppressor cylindromatosis (CYLD) acts as a negative regulator for toll-like receptor 2 signaling via negative cross-talk with TRAF6 AND TRAF7. J. Biol. Chem. *280*, 41111–41121.

Zhang, J., Stirling, B., Temmerman, S.T., Ma, C.A., Fuss, I.J., Derry, J.M., and Jain, A. (2006). Impaired regulation of NF-kappaB and increased susceptibility to colitis-associated tumorigenesis in CYLD-deficient mice. J. Clin. Invest. *116*, 3042–3049.

Zhong, S., Fields, C.R., Su, N., Pan, Y.X., and Robertson, K.D. (2007). Pharmacologic inhibition of epigenetic modifications, coupled with gene expression profiling, reveals novel targets of aberrant DNA methylation and histone deacetylation in lung cancer. Oncogene *26*, 2621–2634.